POLITECNICO DI TORINO
Repository ISTITUZIONALE

A new real-time debris flow and snow avalanche detection system based on optical fiber sensing

Original
A new real-time debris flow and snow avalanche detection system based on optical fiber sensing / Barla, M., Aiassa, S., Antolini, F., Insana, A., Gaudino, R., Rizzelli Martella, G., Pellegrini, S.. - In: LANDSLIDES. - ISSN 1612-5118. - 22:5(2025), pp. 1367-1382. [10.1007/s10346-024-02399-2]

Availability:
This version is available at: 11583/2995912 since: 2025-07-17T06:25:54Z

Publisher:
Springer

Published
DOI:10.1007/s10346-024-02399-2

Terms of use:

This article is made available under terms and conditions as specified in the corresponding bibliographic description in the repository

Publisher copyright
Springer postprint/Author's Accepted Manuscript

This version of the article has been accepted for publication, after peer review (when applicable) and is subject to Springer Nature's AM terms of use, but is not the Version of Record and does not reflect post-acceptance improvements, or any corrections. The Version of Record is available online at: http://dx.doi.org/10.1007/s10346-024-02399-2

(Article begins on next page)

05 November 2026

A new real-time debris flow and snow avalanche detection system based on optical fiber sensing

Marco Barla[a], Santina Aiassa[b], Francesco Antolini*[b], Alessandra Insana[a], Roberto Gaudino[c], Giuseppe Rizzelli Martella[c], Saverio Pellegrini[c]

[a] *Department of Structural, Building and Geotechnical Engineering (DISEG) - Politecnico di Torino, Corso Duca degli Abruzzi 24, 10129, Torino (Italy).*

[b] *Geosolving srl, Corso Orbassano 336, 10137 Torino (Italy).*

[c] *Department of Electronics and Telecommunications (DET) – Politecnico di Torino, Corso Duca degli Abruzzi 24, 10129, Torino (Italy*).

* Corresponding author: francesco.antolini@geo-solving.com, Tel: +39 328 5421340

Abstract

This paper presents a novel real-time detection and early warning system for debris flow and snow avalanches based on distributed optical fiber sensing called Optialp. The functioning principle of the system is based on detecting the vibrations and the impacts generated by the propagation of these phenomena in a spatially continuous way through the real-time analysis of the polarization variations along the optical fibers. A prototype of the system was extensively tested through an experimental laboratory setup reproducing a slope to scale. A series of tests were carried out emulating mass movements. Data recorded from all the tests were used to develop a new algorithm based on a threshold value and a moving average filter capable of distinguishing the signals related to the emulated mass movements from all the further noisy signals. The algorithm was integrated into a prototype of a fiber optic interrogator which performs the real-time analysis of the data acquired and can generate a warning signal whenever mass movements are detected. The results obtained at the laboratory scale have revealed that the technique could precisely, simply, and rather economically identify the polarimetric perturbations induced on the optical fibers by external forces. The laboratory results are promising and suggest that the optical fibers embedded into the ground along one or more sections of the channels where the debris flows or snow avalanches propagate can be used as a novel distributed detection and early warning system, improving the current technologies typically based on discrete monitoring points and sensors.

Keywords: Early Warning, Debris Flow, Snow Avalanche, Detection, Distributed Optical Fibers.

1 Introduction

In the last years, the frequency and the spatial distribution of rain and snow precipitation have drastically changed in many areas of the world accompanied by a simultaneous increase in the frequency of intense phenomena (IPCC 2023; EEA 2017; Stocker et al. 2013, Insana et al. 2021). Debris flows and avalanches are natural phenomena occurring as a consequence of intense or prolonged rainfalls and snowfalls propagating along river catchments and slopes in mountainous regions. Despite the intrinsic differences among the materials involved as well as the different mechanical and rheological features, the commonalities of both these two mass-moving phenomena are:

- the capability to move very quickly i.e. 10 m/s and more (Arattano and Marchi 2005; Bertolo and Wieczorek 2005; Gauer 2014; Havens et al. 2014; Prochaska et al. 2008; Rammer et al. 2007);
- the capability to travel for long distances i.e. up to some km (Butler and Malanson 1992; Hungr et al. 2014; Iverson 1997; Jakob 2005; McClung and Schaerer 2006; Schweizer et al. 2021) from the point where they originate which generally corresponds to the upper portion of a catchment basin or a slope;
- the capability to entrain further materials (soils, rocks, trees) through erosion of the channels and the slopes during the movement;
- their intermittent (or sporadic) occurrence as a consequence of intense rainfalls and snowfalls i.e. prolonged inactivity followed by a sudden recovery;
- a generally high destructive power.

Although the frequency of occurrence of debris flows and avalanches show differentiated trends in different basins that are not easily generalized to a larger scale (Beniston et al. 2011; Bigano and Pauli 2007; Marchi et al. 2002; Pelfini and Santilli 2008; Sass and Oberlechner 2012; Stoffel and Huggel 2012), this frequency in the anthropized basins like the Alpine ones is sufficient to create conditions of high risk for people settlements, road, railways as well as other linear infrastructures exposed to risk. To mitigate this risk, non-structural measures, i.e., monitoring and Early Warning Systems (EWSs) are assuming greater importance thanks to the growing reliability of sensors and transmission systems and their relatively low cost. The aim of the non-structural measures for the mitigation of debris flows and avalanches here considered is primarily to generate timely alarms to be sent and dispatched to all the stakeholders and to the elements exposed to risk through the real-time and continuous observation of physical quantities which characterize the observed phenomenon. A crucial aspect of an EWS is therefore the selection of the most useful quantities to be observed and measured. In this framework, different monitoring systems and techniques for debris flows and avalanches have been proposed (Aaron et al. 2023; Antolini et al. 2019; Arattano and Marchi 2005; Belli et al. 2022; Hurlimann et al. 2019; Itakura et al. 2005; Leonardi et al. 2021; Nagl et al. 2022). Such techniques comprise ultrasonic, radar, and laser sensors for measuring the height of the flow along the channel and the velocity field, seismic and sonic sensors to identify and measure the dynamic effects related to the occurrence and propagation of the mass movements, load cells, force plates, entrainment sensors, sensors for measuring the interstitial pressure of the soil, sensors for identifying the passage of the snow/debris flow or directly installed in the channels where these phenomena usually propagate (trigger lines, wire sensors, pressure sensors, pendulums, clinometers) as well as weather stations to measure the precipitation, video cameras that have more general use, and strain transducers on mitigation structures. In the last years, some remote sensing techniques like the Doppler radar (Gauer et al.

2007; Rammer et al. 2007) and the infrasonic sensors (Thuring et al. 2015; Ulivieri et al. 2011) have also been developed to detect the surface velocities or the air pressure fluctuations related to the occurrence of snow avalanches. The extreme variability of the types of sensors adopted can be noted as well as the fact that no fiber optic system is generally reported in the literature for the monitoring of such phenomena nor for EWS applications.

The applications of optical fibers for geohazard and geoenvironmental monitoring applications date back about 25 years with the attempts at the spatially continuous measurement of some physical parameters such as temperature, deformations, and water content inside earth embankments (Aufleger et al. 1997; Johansson et al. 2000; Beck et al. 2010), followed by applications for monitoring in-depth deformations (Michlmayr et al. 2017; Schenato 2017). Meanwhile, different optical fiber technologies have been developed for geohazard and structural monitoring such as the Optical Time Domain Reflectometry (OTDR), the Optical Frequency Domain Reflectometry (OFDR) both based on Rayleigh, Raman or Brillouin backscattering and the Fiber Bragg Grating (FBG). A more detailed description of the working principles of these techniques is outside the scope of this paper and can be found in Bao and Wang (2021), Bolognini et al. (2009), Hong et al. (2016), Motil et al. (2016). These technologies can be further subdivided into three classes: point, quasi-distributed, and fully-distributed fiber optic sensing (DFOS). The main characteristics, advantages and disadvantages are (Wang et al. 2023):

- point sensing is characterized by a discrete number of sensors that measure changes in parameters in a small area near a predetermined point along the optical fiber line. A typical example is the FBG sensor. They can offer excellent performance in measuring specific locations;
- quasi-distributed sensing contains multiple sensing units to form a sensor array and enables multi-point sensing. The system combines the characteristics of single-point sensors and fully distributed sensors;
- DFOS utilize the fiber to measure physical parameters along its entire length, treating the sensed parameters as functions of the length of the fiber position. This allows DFOS to continuously monitor the external physical parameters distributed along the fiber path, while also obtaining the state of the spatial distribution of the measured physical parameters and their variation over time.

For the real-time detection of avalanches and debris flows DFOS are of particular interest. DFOS are capable of spatially continuous monitoring of the physical parameters of the environment where they are placed, since the “sensor” is made up of the same fibers or set of fibers concatenated together. The mechanism underlying the measurement, which can exploit different processes (Rayleigh, Raman, Brillouin scattering or FBG), is based on a sensor that continuously generates optical pulses that are sent inside the fiber. The variations of the backscattered signal over time measured by the sensor correspond to variations of the properties of the fiber associated to the change of one or more parameters of the environment where the optical fiber is installed. Applications aiming at the high accuracy measurement of stresses, strains, displacements, temperatures, pore water pressures, etc. have been reported in the scientific literature (Inaudi 2014; Lloret et al. 2003; Michlmayr et al. 2017; Olivero et al. 2018; Schenato 2017; Zhu et al. 2017).

The feasibility of the DFOS for the detection of seismic signals related to ice cap microseismicity and more specifically to snow avalanche occurrence has been demonstrated only in the last few years (Edme et al. 2023; Fichtner et al. 2022; Hudson et al. 2021). In particular, in the application described by Edme et al. (2023) a Distributed Acoustic Sensing (DAS) with existing fiber-optic telecommunication cables was used to detect the snow avalanche occurrences in the Swiss Alps.

The preliminary results obtained demonstrated that the proposed system was able to identify their occurrence even though most of them did not reach the fiber optic cable.

On the contrary, very few full-scale applications are known to date concerning the detection of debris flow. For example, Michlmayr et al. (2017) recently confirmed the feasibility of such an approach in the laboratory by carrying out tests in an inclined chute with a distributed acoustic sensing technology based on optical fiber coils. However, the aim of the study was the triggering of shallow landslides caused by the occurrence of intense rainfall and not the detection of snow avalanches and debris flows along a channel. A DFOS-based monitoring system has been developed to measure the impact forces of debris flows directly by Qin et al (2020) and Tan et al. (2020). Whereas, there are no known applications in the literature that envisage the use of DFOS as well as their possible interface with radio nodes for early warning purposes.

Based on the state of the art, the novelty of the current study lies in the investigation of the use of fiber optics for early warning purposes against the occurrence of debris flows and snow avalanches. The motivation stems from the need to tackle the increasing frequency of such events due to climate change and to mitigate the risk for people, structures and infrastructures (Insana et al. 2021). In the following sections, we will present the characteristics of a new system based on the use of fiber optics to detect the propagation of mass movements by measuring in real-time the polarization variations along the whole optical fibers' length together with the result of an extensive laboratory activity aimed at evaluating the feasibility of such system. A preliminary assessment of the technical and economic feasibility of the system for real scale applications is also given.

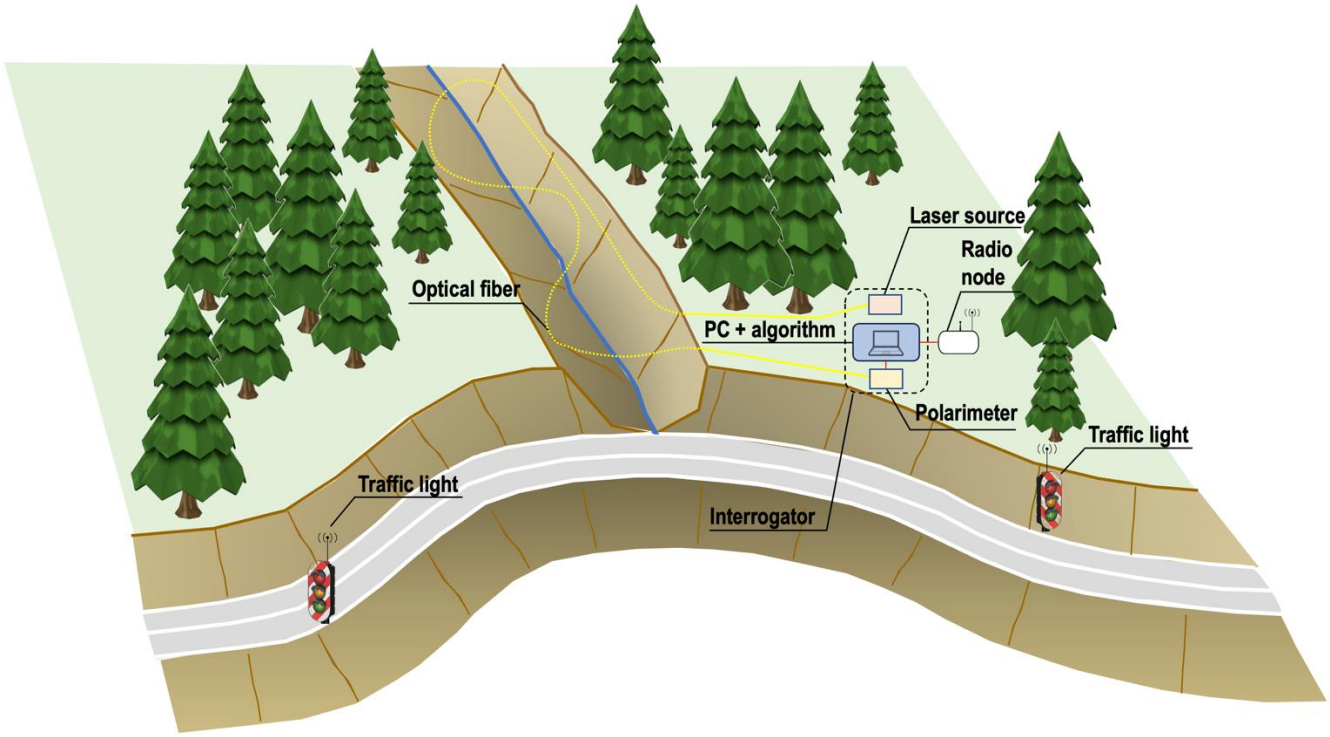
2 Characteristics of the system and principle of operation

The system here described has been submitted to patenting on 07/12/2022 under the number 102022000025158 and will be referred to as Optialp in the following.

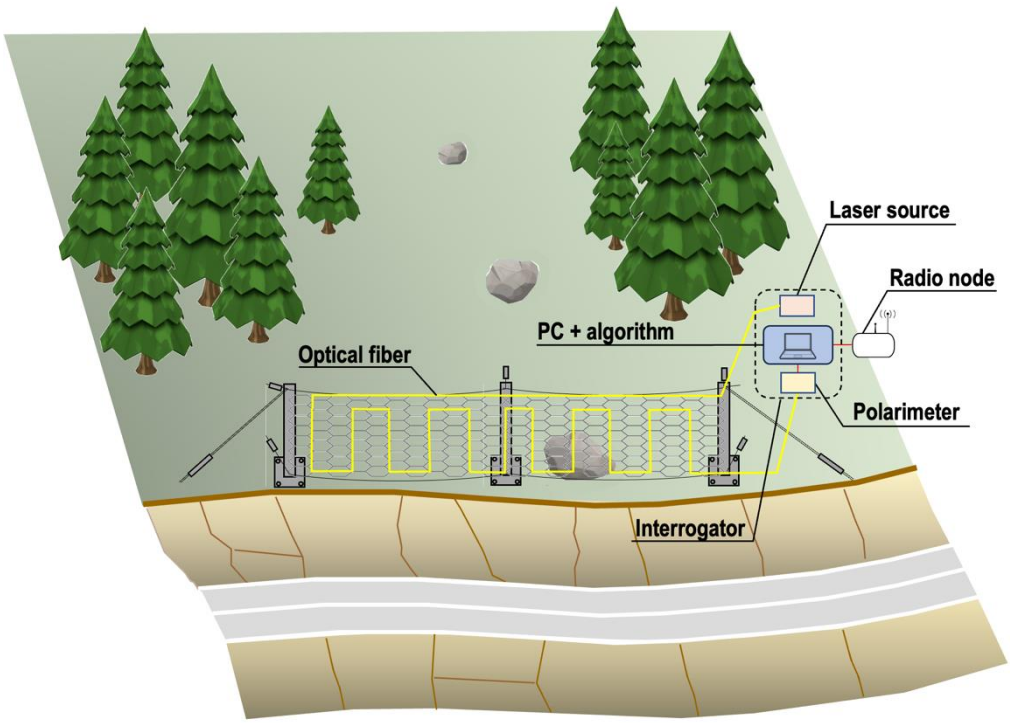
The proposed system to detect mass movements is composed of one or more optical fibers to be installed at the monitored site, connected, at one end, to a laser source and, at the other end, to a polarimeter. The polarimeter will measure data from the optical signal emitted by the laser travelling through the fiber and transfer it to a control unit (a laptop or embedded microprocessor system running a specifically developed algorithm) that can activate, through a radio node, alarm systems such as traffic lights or alternative informative devices to convey specific messages to the elements at risk. Figure 1 shows a schematic layout of the Optialp system in the case of the detection of debris flows and snow avalanches along a channel or to detect the impacts of rock blocks against a rockfall barrier. The optical fiber is buried into the ground along the channel by excavating small trenches to be filled after the deployment of the fibers. Alternatively, they can be directly fixed (by dowels or clamps) to the rock, when present. The first installation mode is more robust, while the second is more prone to damages in case of events. To monitor rock fall impacts, the fibers are hanged to the steel net of the rockfall barrier. Fibers are then physically connected to the so-called interrogator which comprises the laser source, the polarimeter and the control unit.

The detection principle adopted by the system is given by the state of polarization (SOP) of light propagating inside the optical fiber. This can be uniquely described in a three-dimensional space by the Stokes vector ($\vec{S}$), identified by the three Stokes parameters, namely S1, S2, and S3. The three-dimensional space over which $\vec{S}$ is identified is the Poincaré sphere

and each point on its surface represents a different SOP. The state of polarization at a fiber output is affected by birefringence (Forman and Jahoda 1988; Kogelnik and Winzer 2012). External stresses acting on the fibers, such as those generated by mass movements, determine a sudden birefringence variation of the optical material and, consequently, a variation of the SOP of the light propagating inside the fiber. This change can be detected by monitoring the angular variation over time of the Stokes vector called the State Of Polarization Angular Speed (SOPAS). To analyse this, allowing the detection of the physical phenomena occurring, a specific algorithm to be implemented in the interrogator has been developed by the Authors.



(a)



(b)

Figure 1 - Layout of the Optialp system along a gully subjected to debris flows/snow avalanches for road protection (a) and on a rockfall barrier to detect rock blocks impacts (b).

2.1 New algorithm for signals processing

The block diagram of the algorithm developed to process the data acquired from the optical fibers through the polarimeter is shown in Figure 2. The different blocks in the diagram, describe the flow of the interpretation process. Particularly:

- the polarimeter collects the time series of the 3 Stokes parameters;
- using the 3 Stokes parameters collected, the SOPAS is calculated at the instant k;
- a Finite Impulse Response (FIR) filter is applied that carries out a moving average on the input SOPAS values. The output $\omega_s(k)$ is therefore the time-averaged series of the input data. To perform this operation, it is necessary to define the size of the buffer that will contain the samples to be averaged. This value is linked to the T_{mov} parameter, which defines the time duration of the buffer. The greater the moving average window, the greater the buffer to be filled, and therefore the delay introduced in the alarm;
- the output $\omega_s(k)$ values are compared to the SOPAS threshold ω_{th} defined by the user. If the $\omega_s(k)$ value is higher than the threshold, then the alarm is activated.

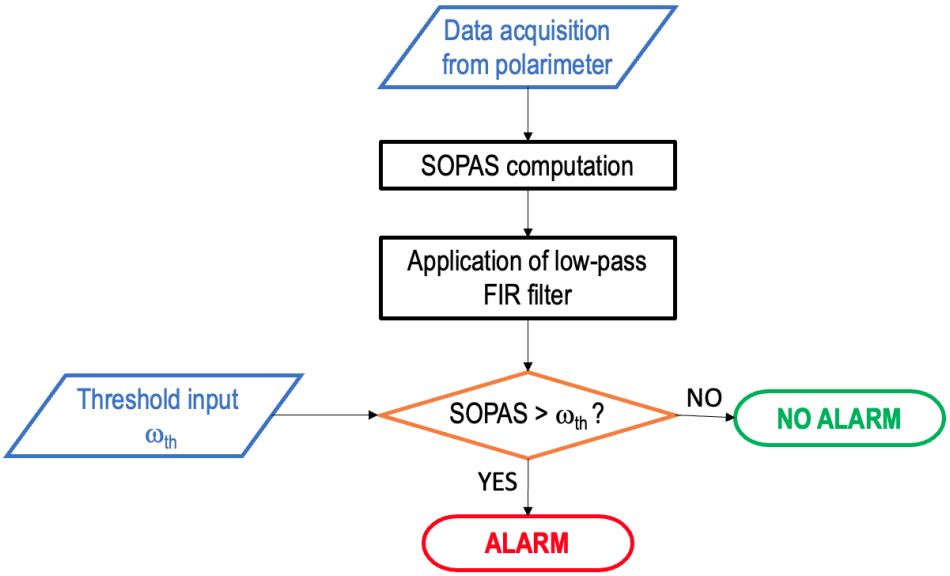


Figure 2 - Blocks diagram of the new algorithm developed to process the signals acquired by the optical fiber and to identify the occurrence of the simulated mass movements.

The low-pass Finite Impulse Response (FIR) filter is applied to eliminate the random peaks i.e., the noise of the measurements, and to smooth the time series. The duration of the time window (T_{mov}) is thus the first free parameter of the algorithm. The other free parameter to be considered in the algorithm is a specific SOPAS threshold value (ω_{th}) expressed in rad/s. Using different combinations of these two parameters, the output of the algorithm could result in a correct detection (CD) of the simulated mass movement, a missed detection (MD) i.e., the simulated event is not detected, or a false alarm (FA) i.e., an alarm is triggered but no event has occurred or another event not related to a mass movement has occurred. In the latter case, further identification and classification of the signals are needed. The FIR filter and the threshold comparison perform a sample-by-sample check of the smoothed SOPAS against the threshold. By increasing the value of T_{mov}, the oscillations in the SOPAS time series reduce, but at the same time, this requires a lower threshold value ω_{th} to be selected to avoid the occurrence of MDs or FAs. The application of higher values of T_{mov} could also introduce an excessive delay in the processing due to the large number of samples contained in the time-moving window. On the contrary, if the threshold value is set too high without accounting for this effect, MD cases are likely to happen; a very low value of T_{mov} does not remove the noise component from the signals and, if the threshold is set too low, FAs might occur. The optimal definition of the two free parameters T_{mov} and the threshold value (expressed in terms of SOPAS) was then evaluated and selected on the basis of the laboratory experimental activity as described in the next chapter.

An in situ implementation of the optical fiber polarization-based monitoring system would be affected by the external environment, e.g. wildlife movements, changing weather conditions, and temperature. Depending on what is considered an hazard and on the noise conditions, the threshold and smoothing filter length value need to be set appropriately through a calibration period on the noise level associated with non-harmful events. Additionally, these events would not generate SOPAS variations overcoming the threshold for an extended period, as debris flow or snow avalanches would. Therefore, a simple upgrade of the algorithm, including a check on the time duration should be enough to distinguish between hazardous and harmless scenarios, reducing false alarm occurrences (Pellegrini et al., 2024).

To further improve the performance of the algorithm, the sampling frequency of the polarimeter was optimized. After a careful analysis of the acquired data in the frequency domain, it was found that the SOPAS variations had frequency components up to a few tens of Hz. Because of this, it was possible to downsample the frequency to 95.4 Hz, the lowest enabled by the polarimeter, therefore reducing the computational effort since this sampling frequency is sufficient to describe and identify the frequency components of the simulated events.

More specific details on the development of the algorithm can be found in Pellegrini et al. (2023, 2024).

2.2 The interrogator prototype

The prototype of the interrogator was obtained by connecting to the optical fiber cable the laser source to one end (out) and the polarimeter to the other end (in). The polarimeter which measures the SOPAS variation along the fiber circuit is interfaced to a PC, where a specific MATLAB script is running in real-time, through a USB connection (Figure 3). The MATLAB script reads with a specific frequency sampling rate equal to 95.4 Hz the Stokes parameters, applies the algorithm described in section 2.1, displays the SOPAS in real-time and generates a specific signal when the SOPAS threshold value is exceeded.

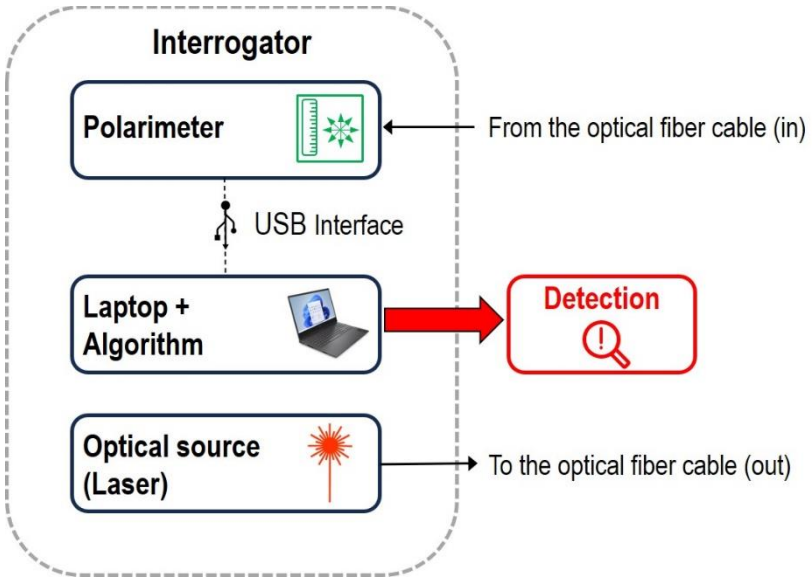


Figure 3 - Scheme of the fiber optic interrogator prototype adopted in the experimental tests.

By coupling the interrogator with a radio node, the output signal generated when the SOPAS threshold is exceeded might be used in an operational environment to control warning tools such as traffic lights which can be placed along mountain roads as shown in Figure 1a.

3 Experimental testing and validation in the laboratory

3.1 Experimental Setup

To test and validate the potential use of the DFOS for debris flows and snow avalanches detection, a scale model of a natural slope was reproduced in the laboratory (**Errore. L'origine riferimento non è stata trovata.**). The model consists

of a phenolic plywood base and plexiglass sides with a size of approximately 3 meters in length and 0.7 meters in width. The plane is made up of two independent parts connected through a series of joint hinges which allow for the independent inclination of the two portions of the plane designed to simulate more articulated geometric configurations of the slope. For the experiments carried out, a uniform inclination equal to about 30° was used. A layer of organic soil mixed with sand, with a total thickness of about 10-12 cm, was placed over the plywood base and inside a geotextile. The latter has the function of protecting the underlying wooden surface, as well as facilitating the compaction of the soil and sand mixture. Buried in the soil, single optical fibers were embedded at three different depths (10, 50, and 90 mm) using three different geometric layouts (Figure 5):

- Parallel to the maximum slope inclination placed in the middle of the model (U_C);
- Parallel to the maximum slope inclination alongside one edge of the model (U_L);
- Transversal to the maximum slope inclination with six transversal crossings (T) placed at a distance comprised between 400 and 500 mm from each other.

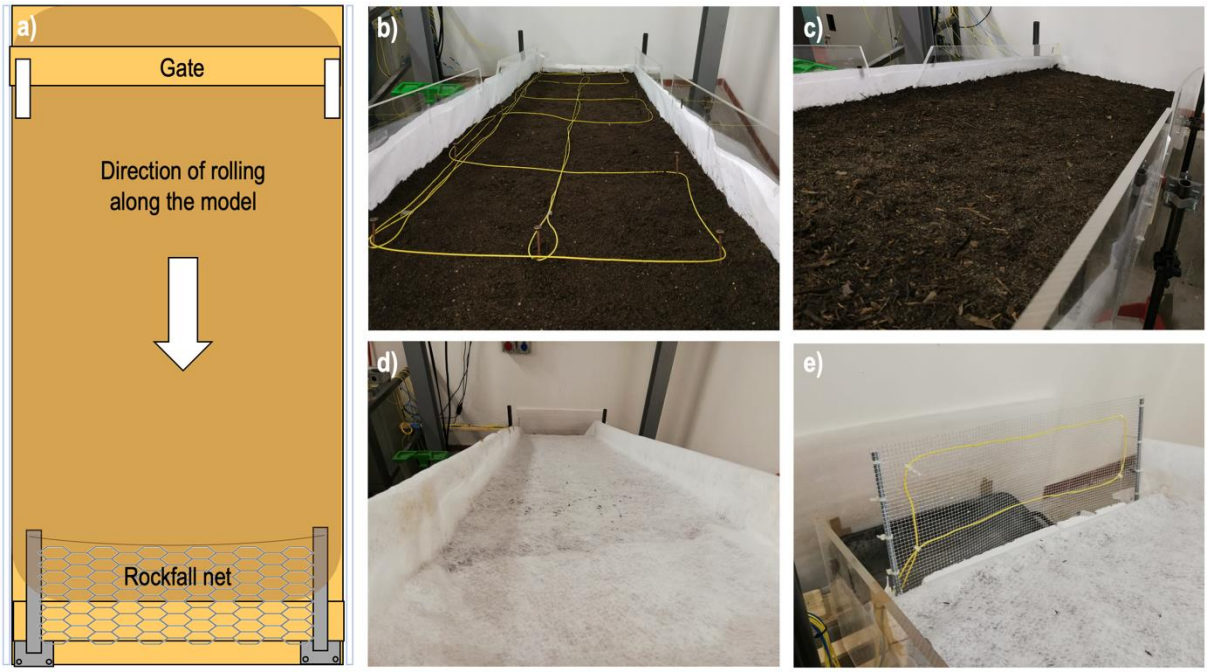
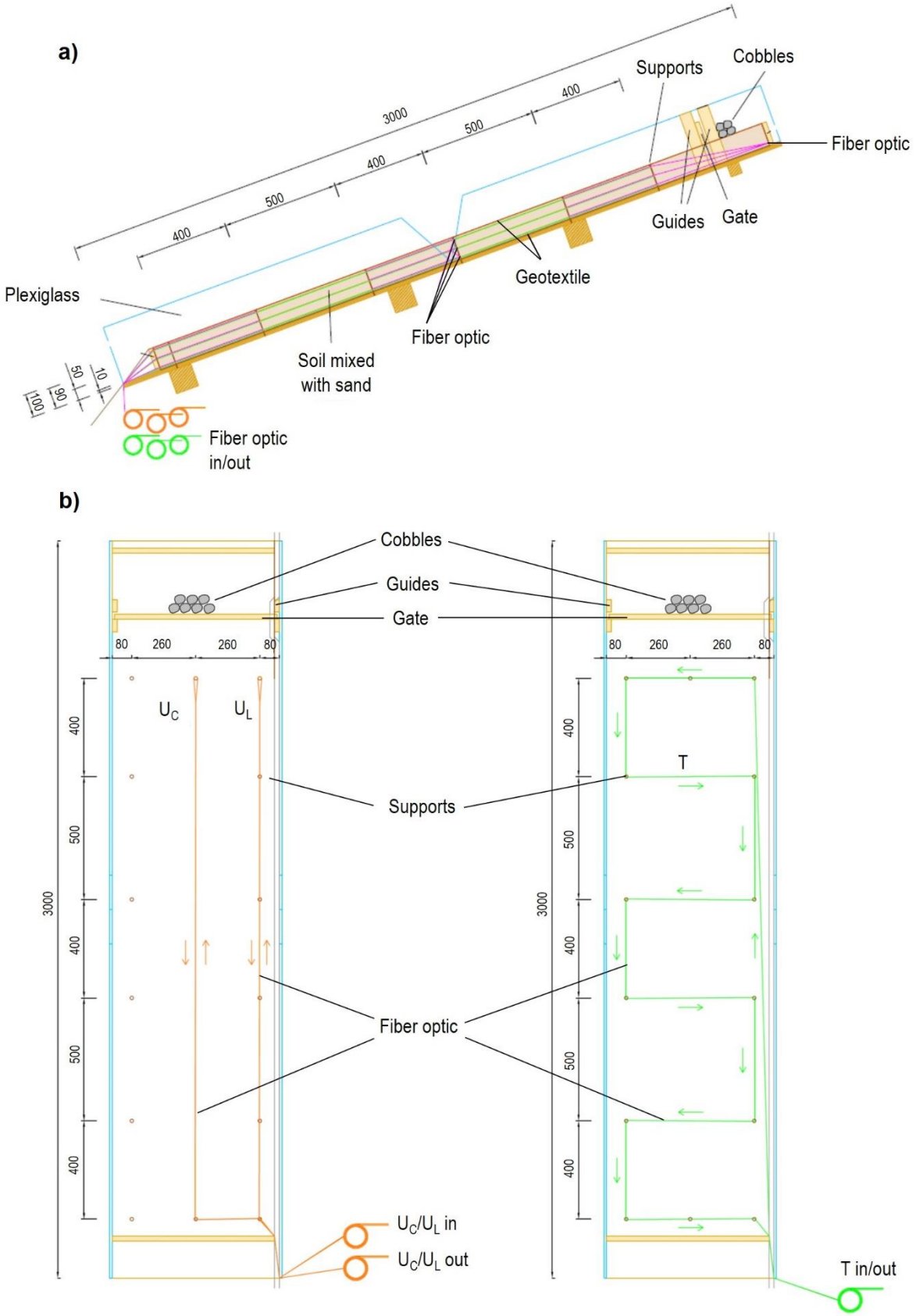


Figure 4 – Sketch of the experimental setup (a) and pictures of the construction phases: installation of the optical fibers (b), covering with soil (c), installation of the protective geotextile (d) and installation of the rockfall net equipped with optical fibers (e).



227

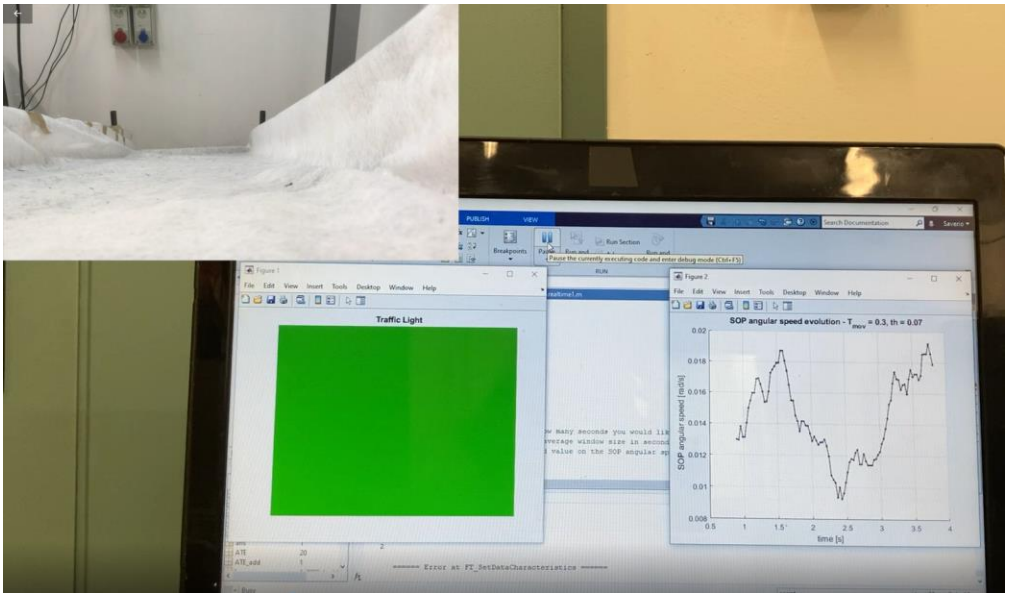
228 Figure 5 – Schematic cross section (a) and plan views (b) of the experimental setup highlighting the arrangement of the

229 different optical fibers layouts.

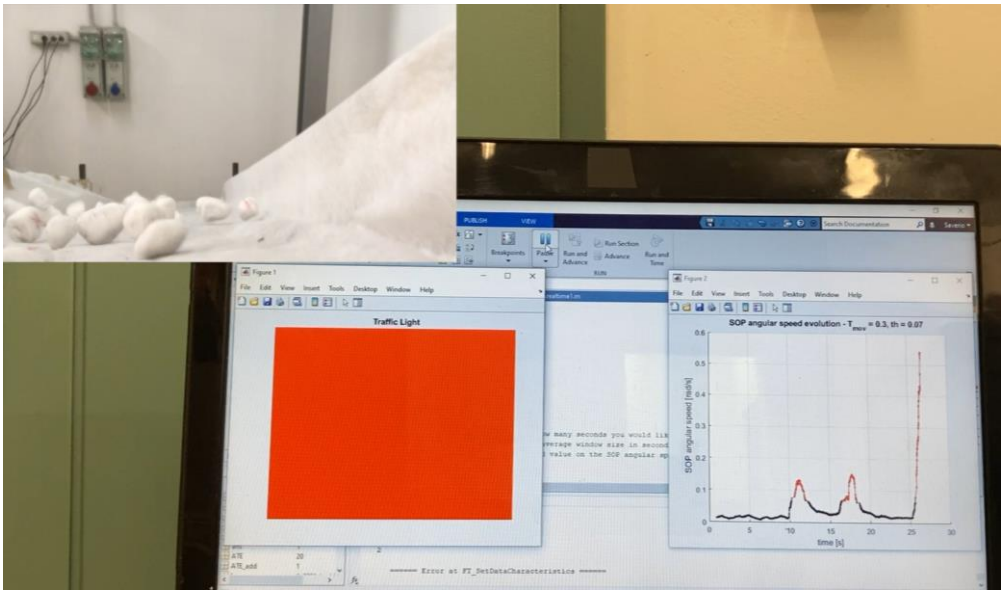
Table 1 summarizes the main geometric characteristics of the different fiber optic layouts installed in the model. A series of rigid supports were used to tie the fibers outside the model thus minimizing possible oscillations that could alter the measurements. The experimental setup model is completed by a wooden liftable gate installed in the top portion of the slope, allowing for the release of different granular materials for simulating mass movements occurring along the slope. Each termination of the optical fibers is connected respectively to a laser and a polarimeter placed at a short distance from the model. A Fabry-Perot laser emitting light at 1550 nm was used as the optical source for the signal propagating inside the single-mode fibers. The optical fibers are then coupled into a laboratory polarimeter (Novoptel PM1000), an instrument that allows measuring with a specific sampling frequency f_s the SOPAS of the light, included in the interrogator prototype described in section 2.2. When the SOPAS threshold is exceeded, an acoustic signal is activated and a red light is turned on to the PC screen (Figure 6).

Table 1 - Summary of the main geometric characteristics and corresponding code of the different fiber optic layouts installed in the laboratory scale slope model.

Geometric layout	**Depth (mm)**	**Code**
Parallel to the maximum slope inclination in the middle of the model	10	$U3_C$
	50	$U2_C$
	90	$U1_C$
Parallel to the maximum slope inclination alongside one edge of the model	10	$U3_L$
	50	$U2_L$
	90	$U1_L$
Transversal to the maximum slope inclination with six transversal crossings	10	T3
	50	T2
	90	T1
Rockfall net – simple loop	-	RN1
Rockfall net – meandering loop	-	RN2



(a)



(b)

Figure 6 – Operation of the optical fibers interrogator and emulation of a traffic light on a PC screen: when operating below the SOPAS threshold value and no events are identified (a) and when the SOPAS threshold value is exceeded and the alarm is triggered (b).

3.2 Testing program

More than 1500 experimental tests were performed, measuring the variation of the SOPAS along the fibers installed inside the physical model. The following conditions, which take into account different mobilized volumes and materials were reproduced:

1. No mechanical perturbation, to characterize the noise level of the system (N - Noise);
2. Rolling of one rock cobble (diameter equal to 4 cm) along the slope (S – Stone);
3. Rolling of a plastic cylinder (15 cm long and 5 cm in diameter) along the slope (C – Cylinder);

4. Release of different amounts of cobbles (13-25 pieces with an approximate diameter of 4-5 cm) along the slope (DF – Debris Flow);
5. Rolling of one cobble (approximate diameter 4 cm) along the slope and final impact against a rockfall net equipped with fiber optic (RN – Rockfall Net).

The assumption that has been made in this work is that the three different harmful events (debris flow, cylinder, single rock) are to be detected by the algorithm. The latter condition (DF) tries to reproduce, to scale and without the use of water, the occurrence of a mass movement along a slope or a channel which can be comparable to scale to the dynamic signal produced by a debris flow or a very dense avalanche (i.e. wet snow). The duration of the tests is variable, lasting from a minimum of 10.75 to a maximum of 21.5 s, in order to capture the whole evolution of the simulated events. The cylinder (C) and single rock (S) events have been selected with the aim to test the capability of the algorithm to detect them, as well as to understand the magnitude of the SOPAS in the different cases and to calibrate the algorithm parameters.
For each optical fiber tested (U_C, U_L, and T), the measurements of the noise level of the system were performed at least three times, while the other conditions (S, C and DF) were tested at least ten times. This subset of 33 tests, which was repeated many times, was adopted to evaluate the possible variations of the noise levels over time and to easily identify possible sources of disturbances on the experimental setup.
Some long-term noise measurements (several hours) were also carried out to verify the presence of any deviation and potential anomalous behaviours of the noise over time. The test's repetition made it possible to create a sufficiently large database of signals which could be used to classify and distinguish the signals related to the emulated mass movements from all the further noisy features.

3.3 Results of the laboratory tests

The result of each test after the signals processing can be expressed through graphs showing the variations over time of the SOPAS angular speed in radians per second. Figures **7**, **8** and **9** show the results of a series of tests both for the three different optical fibers configurations U_L, U_C and T installed at different depths in the model (90, 50 and 10 mm) and for each test type carried out (S, C, DF and N). To allow a fruitful comparison, all scales' range are the same. Figure 10 shows the results for the tests carried out adopting the configurations RN1 and RN2.

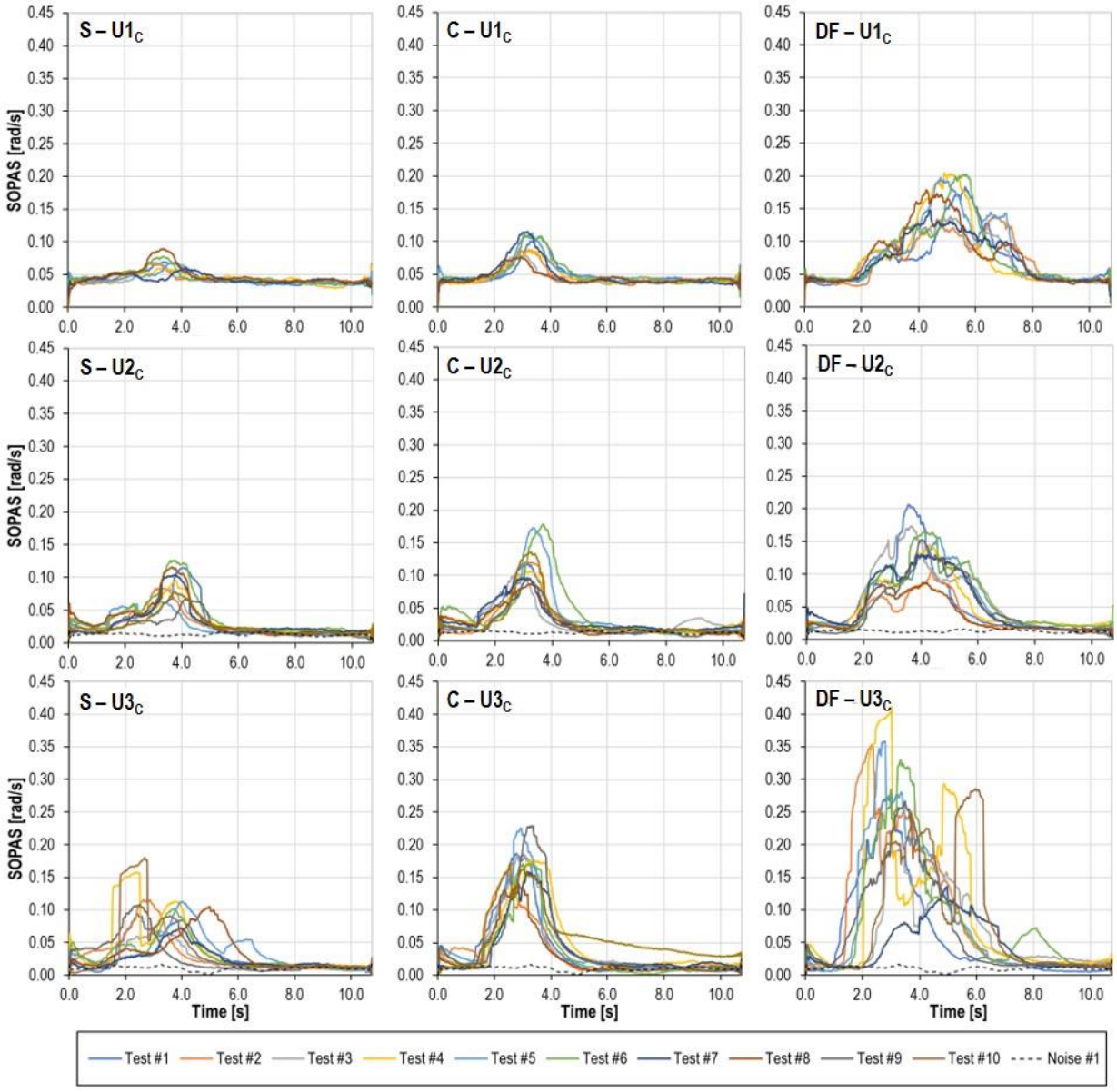


Figure 7 - Experimental results of 86 tests using the U_C optical fibers configuration compared to noise measurements when available. The different codes identify the test carried out (S, C, DF) and the depth of the optical fibers in the model (1 = 90 mm, 2 = 50 mm, 3 = 10 mm).

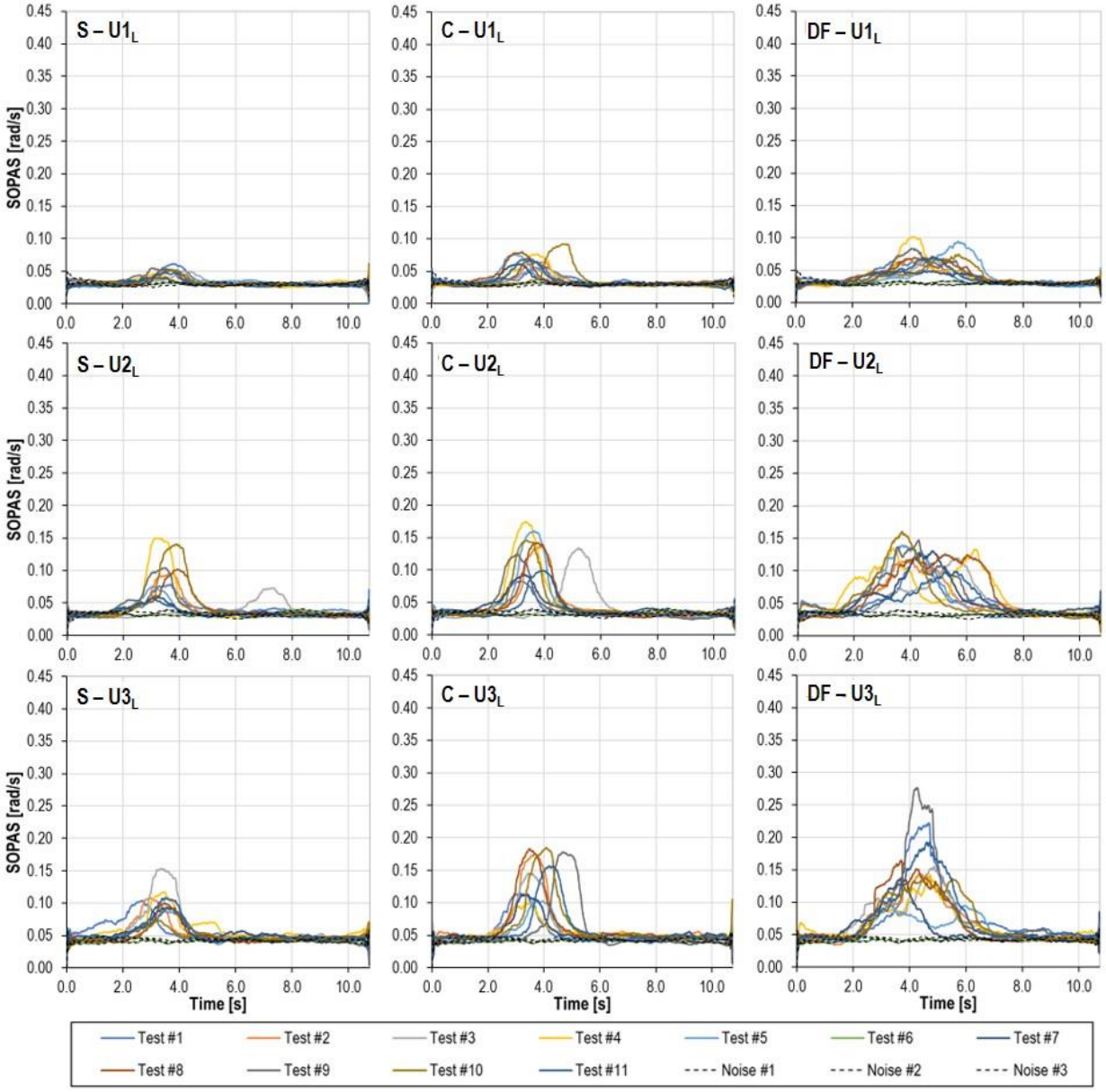


Figure 8 – Experimental results of 108 tests using the U_L optical fibers configuration compared to noise measurements. The different codes identify the test carried out (S, C, DF and N) and the depth of the optical fibers in the model (1 = 90 mm, 2 = 50 mm, 3 = 10 mm).

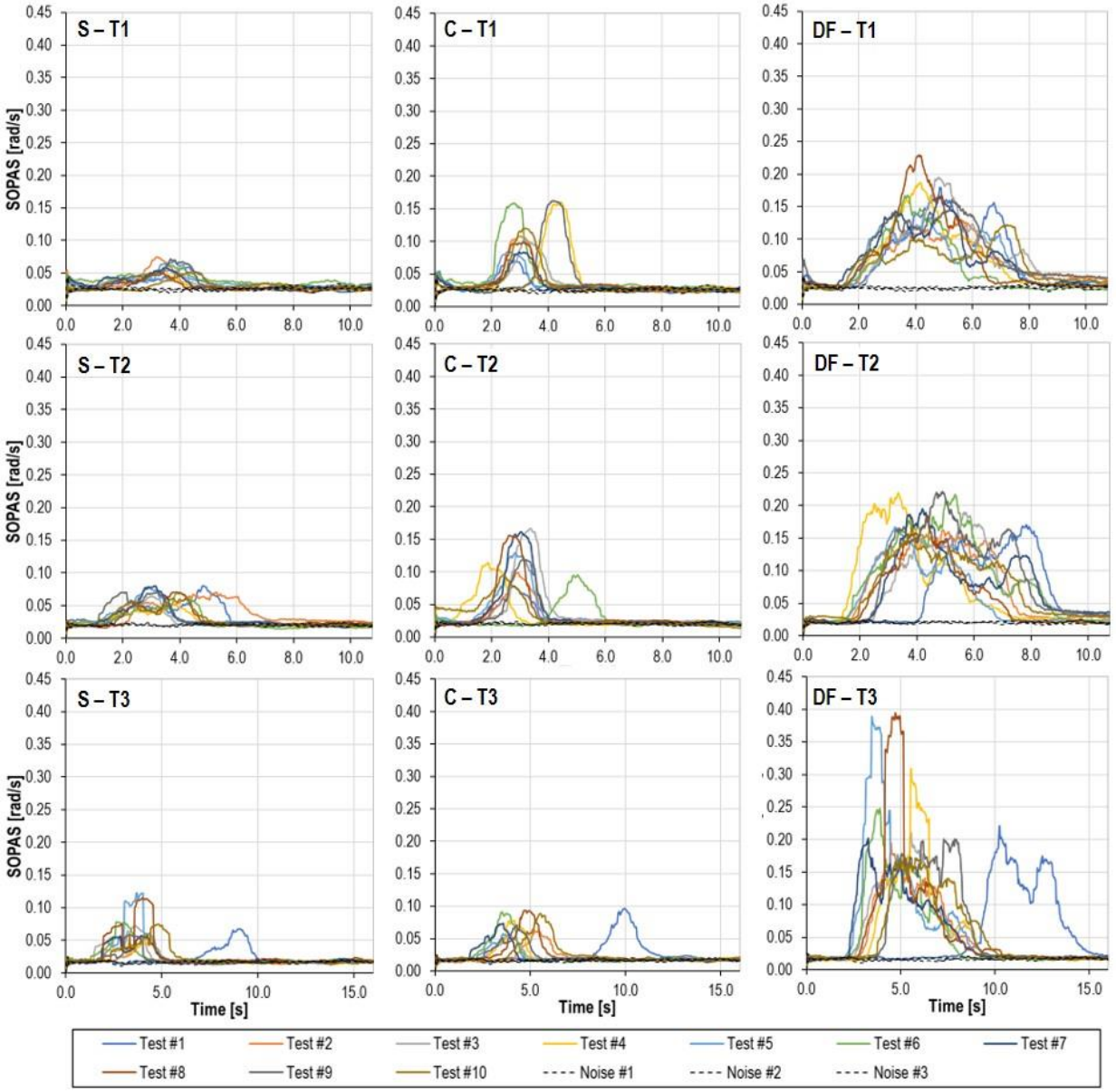


Figure 9 – Experimental results of 99 tests using the T optical fibers layout compared to noise measurements. The different codes identify the test carried out (S, C, DF and N) at a depth of 90 mm (1), 50 mm (2) and 10 mm (3) respectively.

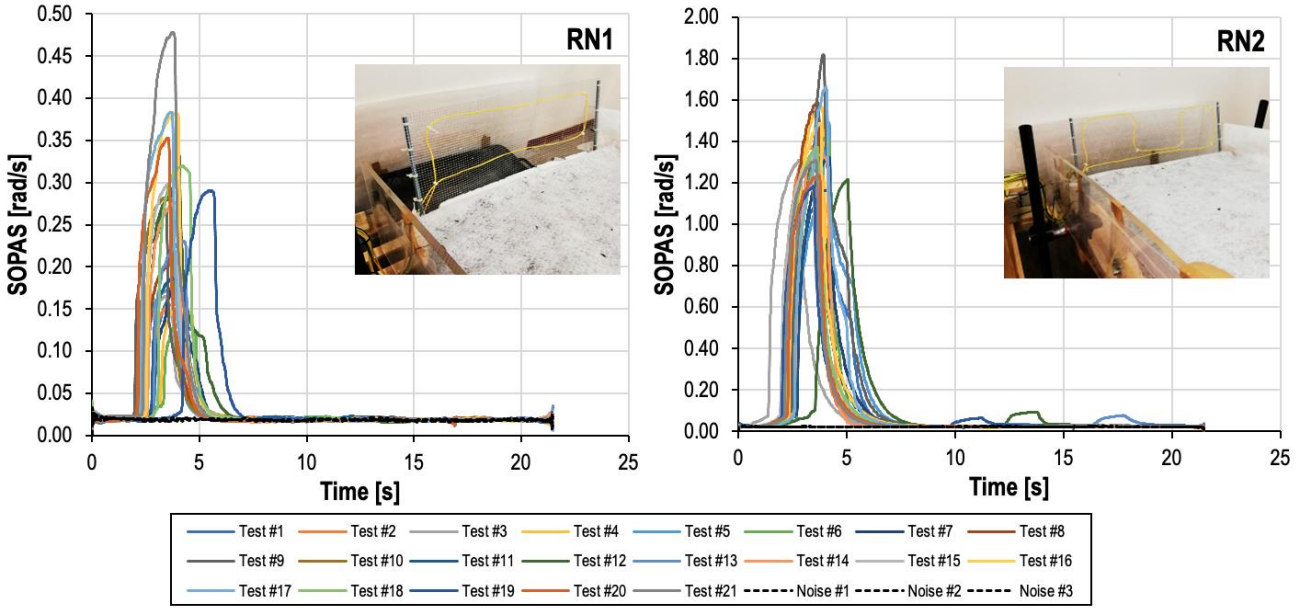


Figure 10 – Experimental results of 48 tests using the RN1 and RN2 optical fibers layout compared to noise measurements.

All graphs show initially low SOPAS values, comparable to the measured noise levels, followed by a rapid increase up to one or more peaks, followed by a gradual decrease to the initial conditions when the simulated event is over. In general, the N simulations highlight noise levels (i.e. SOPAS values lower than 0.05 rad/s) that are comparable among the U_L, U_C, T and RN layouts tested without any significant differences.

The time series of S and C simulations are characterized by smoother patterns which reflect the dynamics of a single object rolling along the model. The DF time series are instead more complex and articulated since they reflect the dynamics of a granular media composed by macroscopic particles where collisions and rebounds take place in addition to rolling. It is also evident that the maximum SOPAS values were measured for the DF tests followed by the C and S tests for all the three different installation depths of the optical fibers. In some cases, as for instance the $U2_L$ and T3 layouts, the C and S tests have given comparable maximum SOPAS values. This can probably be related to the similar masses and velocities of the falling objects used in these tests.

The results of all the tests have been summarized in Figure 11 with the aim to have a glance at the statistical distribution of the test results. Here it can be seen that, given the randomness of the tests carried out, the results obtained in terms of maximum SOPAS change every time, however the order of magnitude of the maximum SOPAS recorded is always the same and in general higher than the recorded noise. This testifies the repeatability and reliability of the tests, despite the variability related to the testing conditions that shows that the DF condition, the most representative for in situ events, always stands out with respect to the others. In general, Figure 11 shows that the higher the depth of installation of the optical fibers, the lower the maximum SOPAS values measured during both S, C and DF tests. Also, the configurations RN1 and RN2 that simulate the rockfall barrier application are both effective, though the second one, due to its particular geometry, leads to much higher values of maximum recorded SOPAS.

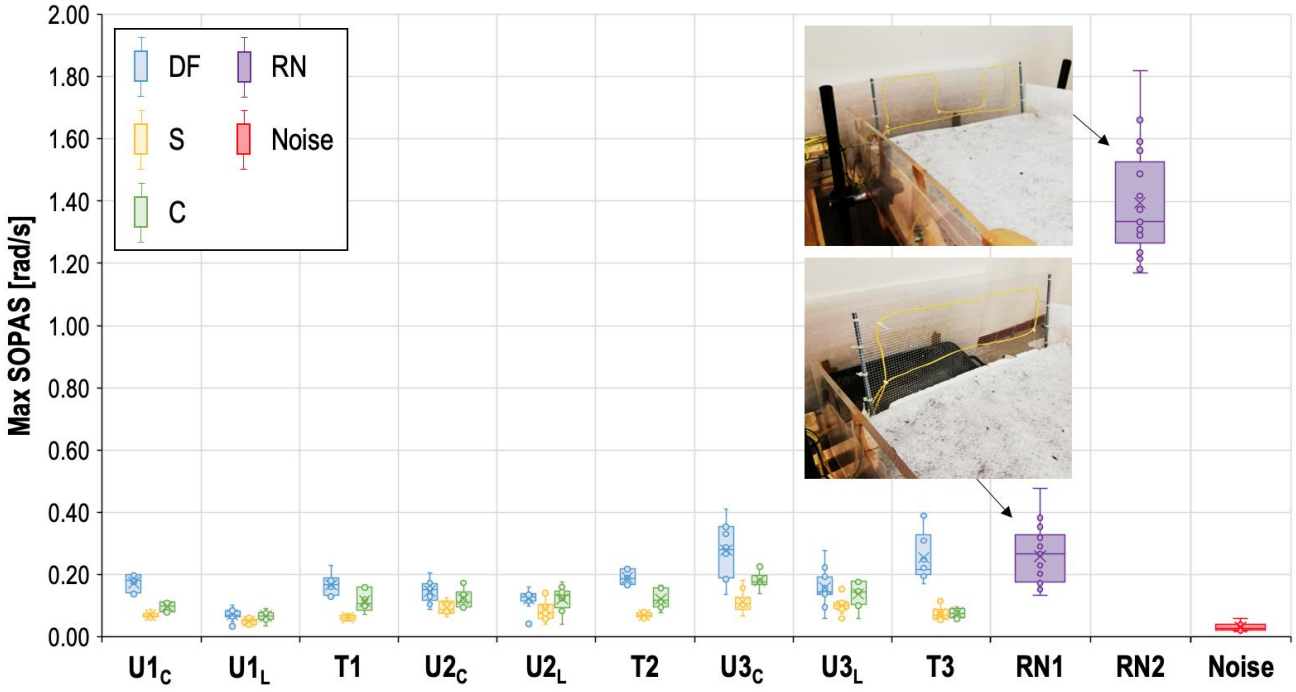


Figure 11 – Maximum SOPAS measured in all the tests carried out with the eleven different fibers optic layouts Uc, U_L, T (at a depth of 90 mm (1), 50 mm (2) and 10 mm (3) respectively), RN1 and RN2, and at rest (noise).

Through the analysis of the SOPAS time series, it was also possible to estimate the average velocity of the falling objects along the experimental slope model. The values obtained are consistent with the time recorded during the experiments and appear to be in the range 0.9-1.9 m/s for the S and the C tests and 0.6-0.8 m/s for the DF tests. It is interesting to note that debris flows in alpine catchments are generally characterized by moderate propagation velocities of less than 10 m/s that can reach a lower bound values close to 1.5-2.0 m/s (Arattano and Marchi 2005; Coviello et al. 2019; Hurlimann et al. 2003; Schimmel et al. 2022).

The results obtained have shown that for all three optical fiber geometric layouts (U_C, U_L, and T) and the different depths of installation tested, the system was able to sense and measure the SOP variations along the optical fibers caused by the vibration which propagates in the soil during the simulation of a mass movement at the laboratory scale. It is also shown that the detection occurs better for the fibers closer to the surface, however also the deepest ones are able to detect the event.

3.4 Validation of the algorithm

To assess the performance of the algorithm, all the data collected during the experimental campaign were processed through the application of the detection algorithm. The result obtained can be represented by specific contour plots which show, for each test type carried out (S, C, and DF), different combinations of T_{mov} and ω_{th} values.

The graphs in Figure 12 summarize the behaviour of the algorithm for the three configurations of the fibers tested (U_C, U_L, and T) in all the 1500 tests performed. The green colour identifies a 100% correct detection (CD) rate on all fibers, regardless of their depth and for all the simulated mass movement events, while the red colour identifies pairs T_{mov}-ω_{th} for which there

is a lack of identification (MDs and/or FAs). The lack of identification may depend either on the fact that the noise level is higher than the threshold or because at least one of the simulated events remains below the threshold for its entire duration. Yellow or orange colours denote intermediate conditions i.e., using these parameters the algorithm is able to correctly identify the simulated mass movement in the experimental model for some cases only. The layout of the plots, in terms of arrangement and distribution of the areas, suggests that a wide range of T_{mov}- ω_{th} values can be used in the algorithm to obtain always a correct detection of the simulated events.

In particular, the system proved to be able to correctly recognize the mass movements from the condition of noise only and from further random disturbances simulated. This ability has been demonstrated for multiple combinations of the values T_{mov}- ω_{th} that, after an appropriate optimization, can be used in the real-time detection algorithm. For instance, by analyzing the overall results shown in Figure 12**,** values of T_{mov} in the range 1 – 2 s coupled with thresholds values between 0.035 and 0.045 rad/s allowed for a correct triggering of the alarm regardless of the fibers installation depth. Even the position of the optical fibers in the model (central, lateral, or transversal) does not seem to be relevant for the detection of the simulated mass movements as shown in Figure 12. This has a very important implication for a future application of the system outside the laboratory. Although at the site scale it is realistic that the vibrations related to debris flows and snow avalanches may differ from those simulated in the laboratory, it is expected that the ratio between the environmental noise and the signal generated by these events may be similar since the optic fibers will be installed in the ground at depths greater than those tested in the laboratory. The determination of the T_{mov} and ω_{th} values to be used on a real site, would require a recalibration to identify the SOPAS thresholds which could be sensibly higher.

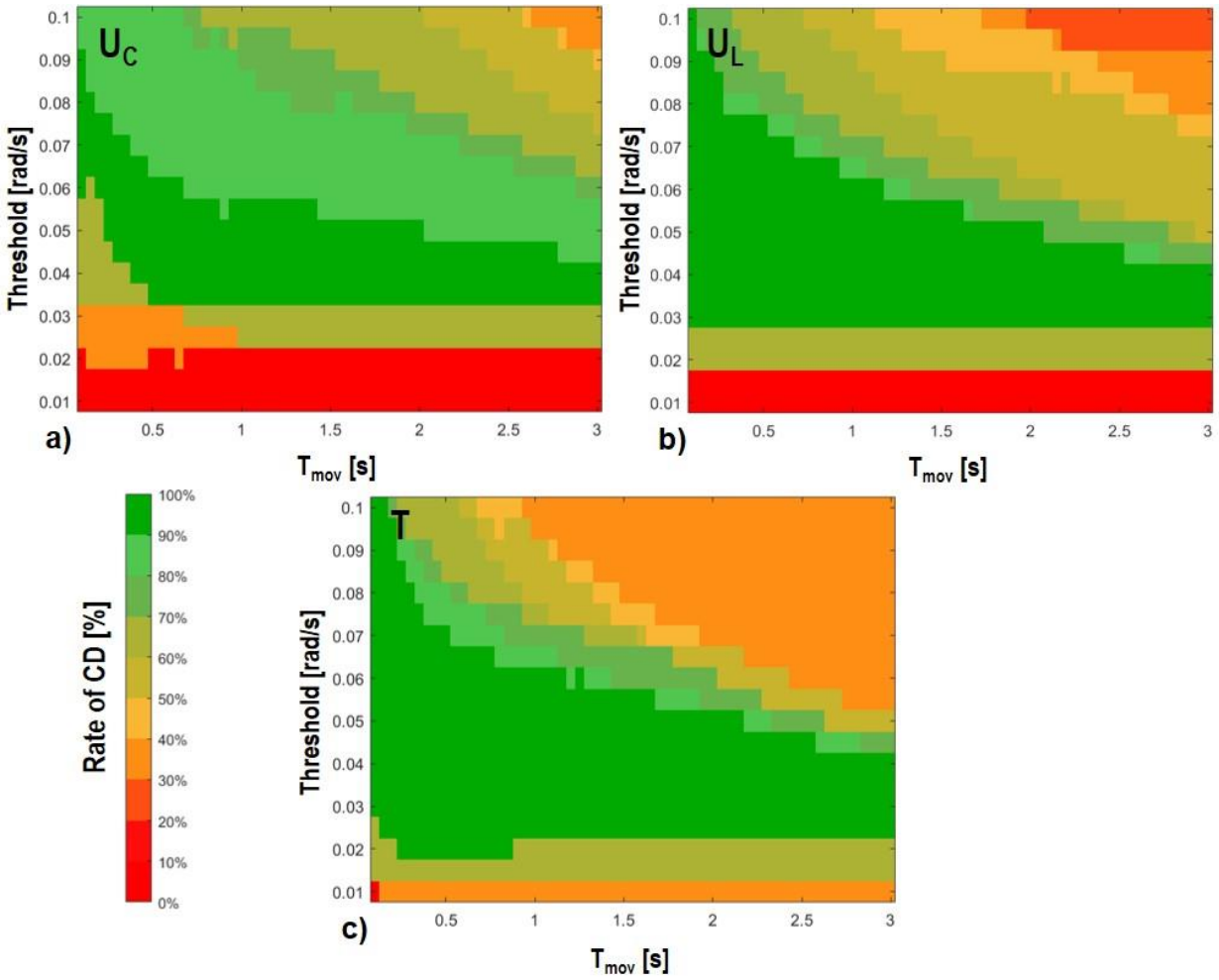


Figure 12 - Contour plots showing the overall behaviour of the algorithm adopted to process the signals in terms of rate of correct detection (CD) for the three configurations of the fibers tested U_C (a), U_L (b) and T (c) and for all the three depths of installation (1 = 90 mm, 2 = 50 mm and 3 = 10 mm) with the variation of the time moving average (T_{mov}) and the State of Polarization Angular Speed (SOPAS) threshold ω_{th}

The previous observations are also extremely interesting for identifying the best installation geometry of the optic fibers: for instance, by adopting a scheme where the optic fibers will be installed alongside of a channel (similar to the U_L scheme previously described), it would be possible to correctly identify the occurrence of debris flows and snow avalanches as well as to simplify the installation thus reducing the costs. Furthermore, this installation scheme along with the embedment of the fibers into the ground will significantly minimize the possibility of damages to the sensing system (therefore minimizing maintenance) since the cables will not interact directly with the masses moving along the gullies. In any case, should the optical fibers be damaged, it will be possible to repair them easily on site through a partial replacement of the cables or through a splicing.

4 Assessment of the technical and economic feasibility of the system

The technical analysis of the proposed monitoring system based on optical fiber has highlighted excellent experimental results after an appropriate optimization of the free parameters of the algorithm proposed for signals processing and the

subsequent generation of alarms. From a technological point of view, the results obtained so far have identified how the optical fibers polarimetric measurement constitutes an extremely promising technique in the geological and geotechnical fields since it has shown to be able to identify in a precise, prompt and rather simple way the polarimetric perturbations induced on the optical fibers by external forcings.

From an economic point of view, considering, for instance, an optical fiber loop of about 1 km installed along a mountain slope, the cost for the different devices (fiber optic cable, laser, polarimeter with an embedded real-time data analysis system, stand-alone power supply and radio node) is approximately around 25,000 €. Most of the cost is for the interrogator system, while the fiber optic cables would cost less than 2000 €. To this amount, the costs of the deployment of the optical fibers into the ground have to be added. These can vary depending on the ground to be excavated and the subsequent backfilling technique adopted and can be reduced if the fiber cable is fixed to the rock surface. An additional cost of approximately 5,000 € can be estimated to install the optical fiber at a depth of 5-10 cm, less in case of surface deployment. This will lead to a total cost of around 30,000 € for the deployment and installation of an EWS system based on the proposed technique.

The estimated cost is slightly higher than typical installation costs for EWS systems based on "discrete" sensors (such as trigger lines, ultrasonic, seismic, or infrasonic sensors, etc.). However, it is believed that the technical advantages that is acquired with the use of a DFOS system can compensate for the higher installation costs. The possibility to measure data over large areas where the debris flows or the avalanches propagates and to transfer this information through fiber optic cables at distance from the monitored area is a peculiar aspect. Another value-add of the technique is the possibility to measure the velocity of the snow and debris masses moving along channels and slopes by using different optical fiber circuits placed at different positions along the channel coupled with an optical switch (i.e. using the same interrogator). The optical switch allows to interrogate sequentially and in real time all the circuits to identify the passage of a snow or debris mass in different channel sections. The signal retrieved by each circuit combined with the specific position along the slope may be then used to calculate the velocity of the moving mass. Finally, the reliability of the detection algorithm and the reduction of false alarms could also increase safety along roads or railways reducing unnecessary closure to the transit of the infrastructure or, worse, the direct involvement of the users of the infrastructures. There are also potential long-term savings from reduced maintenance in comparison with other systems (e.g. no need to adjust pendulums height for winter and summer detection, less elements at risk of damages during strong events).

5 Conclusions

A new system, called Optialp, to detect the propagation of debris flows and snow avalanches along mountain gulleys and generate alert signals to be used in an EWS was here presented. It is applicable to mountain gullies where debris flow phenomena and/or snow avalanches occur repeatedly over time with similar intensity and kinematics as well as on rockfall hazard mitigation structures. The proposed system is reliable, simple, and requires quite low-cost devices.

The main focus of the work was to demonstrate the effectiveness of the system by presenting the results of an extensive laboratory activity aimed at evaluating the feasibility of the use of a new DFOS system to detect the propagation of simulated mass movements by measuring in real-time the polarization variations along the optical fibers. The results obtained have

identified how the measurement of optical fibers polarimetric variations can identify, at least at the laboratory scale, in a precise and rather simple way the polarimetric perturbations induced on the optical fibers by external forcings. The performance of the system for the identification of the simulated mass movements in the model is satisfactory after an appropriate optimization of the free parameters (T_{mov} and ω_{th}) which govern the algorithm developed for the processing of the signals and for the subsequent generation of alarms. At the same time, the algorithm characterized by a high speed of response has shown a minimization of the probability of occurrence of false alarms or missed detection. The algorithm is embedded into a prototype of the fiber optic interrogator capable to perform the real-time analysis of the acquired data and to generate an alarm signal whenever the threshold value of the state of polarization angular speed (ω_{th}) is exceeded.

The examination of the economic feasibility of the system highlighted slightly higher construction and installation costs with respect to existing alternatives based on "discrete" sensors. Nevertheless, this can be considered acceptable considering the advantage of being able to measure and detect mass movements along large sectors of slopes or catchment basins. It is believed that the technical advantage that is acquired with the use of Optialp can completely compensate for these initial slightly higher costs. Moreover, the possibility to carry out a distributed measurement, extending the sensing system for lengths even greater than few kilometers, rather than the use of discrete sensors for large-scale linear infrastructures determines a better and higher mitigation of the risks caused by debris flows and avalanches.

The laboratory results suggest that the optical fibers embedded into the ground along one or more sections of the channels where the debris flows or snow avalanches propagate can be used as a novel distributed detection and early warning system, improving the current technology which typically is based on discrete monitoring points and sensors. The Optialp system could then represent a valid alternative to the existing state-of-the-art monitoring techniques, both in the geotechnical and optical fields. The instantaneous and real-time response and the high sensitivity of optical fibers coupled with a high wear resistance of the cables embedded into the ground and relative ease of installation are all value adds. From the optical point of view, the advantages of the polarimetric technique adopted for the Optialp system are the simpler and therefore less expensive equipment than other DFOS based on OTDR, OFDR and FBG as well as the simpler processing required to identify debris flows and avalanches.

Further experimental activity will be devoted to testing the system in a relevant environment i.e., a gully where debris flows and/or avalanches usually occur, to confirm the satisfactory results obtained at the laboratory scale and verify the robustness of the installation. The use of artificial intelligence based on neural networks could also be investigated to automatically identify the change of polarization along the fibers related to the occurrence of real debris flows and avalanches and to distinguish among different events, enabling not only a further reduction of the false alarms and missed detection cases but also a classification of the events.

Acknowledgements

The work described in this paper was partially funded by Regione Piemonte under the P.O.R. FESR 2014/2020 – Asse I – Azione I.1b.I.2 Bando PASS “OPTIALP Project”. The authors would also like to thank Yihan Du, Daniele Rosi and Filippo Vigna for their help in the experimental setup construction and the execution of the testing program.

Author contributions:

Conceptualization: Marco Barla; Methodology: Marco Barla, Roberto Gaudino, Alessandra Insana; Formal analysis and investigation: Francesco Antolini, Alessandra Insana, Giuseppe Rizzelli Martella, Saverio Pellegrini; Experiments: Francesco Antolini, Marco Barla, Alessandra Insana, Giuseppe Rizzelli Martella, Saverio Pellegrini; Writing - original draft preparation: Francesco Antolini; Writing - review and editing: Marco Barla, Alessandra Insana; Funding acquisition: Santina Aiassa, Marco Barla; Resources: Santina Aiassa, Marco Barla, Roberto Gaudino, Alessandra Insana; Supervision: Marco Barla, Roberto Gaudino.

Competing Interests:

The authors submitted to patenting on 07/12/2022 the system described in the paper (Priority number 102022000025158).

References

Aaron J, Spielmann R, McArdell BW, Graf C (2023) High-frequency 3D LiDAR measurements of a debris flow: A novel method to investigate the dynamics of full-scale events in the field. Geophys Res Lett 50, e2022GL102373. https://doi.org/10.1029/2022GL102373

Antolini F, Aiassa S, Barla M (2019) An Early Warning System for Debris Flows and Snow Avalanches. In: Calvetti F, Cotecchia F, Galli A, Jommi C (eds) Geotechnical Research for Land Protection and Development. CNRIG 2019. Lecture Notes in Civil Engineering, vol 40. Springer, Cham

Arattano M, Marchi L (2005) Measurements of debris flow velocity through cross-correlation of instrumentation data. Nat Hazard Earth Sys 5(1):137-142. https://doi.org/doi_10.5194/nhess-5-137-2005

Aufleger M, Conrad M, Goltz M, Perzlmaier S, Porras P (2007) Innovative dam monitoring tools based on distributed temperature measurement. Jordan J. Civ. Eng 1(1):29-37

Bao X, Wang Y (2021) Recent advancements in Rayleigh scattering-based distributed fiber sensors. Advanced devices & instrumentation. https://doi.org/10.34133/2021/869657

Beck YL, Khan AA, Cunat P, Guidoux C, Artières O, Mars J, Fry JJ (2010) Thermal monitoring of embankment dams by fiber optics. In: Proceedings of the 8th ICOLD European Club Symposium, Innsbruck, Austria, 22-23 September 2010, pp 444-448

Belli G, Walter F, McArdell B, Gheri D, Marchetti E (2022) Infrasonic and seismic analysis of debris-flow events at Illgraben (Switzerland): Relating signal features to flow parameters and to the seismo-acoustic source mechanism. Journal of Geophysical Research: Earth Surface 127, e2021JF006576. https://doi.org/10.1029/2021JF006576

Beniston M, Stoffel M, Hill M (2011) Impacts of climatic change on water and natural hazards in the Alps: can current water governance cope with future challenges? Examples from the European “ACQWA” project. Environmental Science & Policy, 14(7):734-743. https://doi.org/10.1016/j.envsci.2010.12.009

Bertolo P, Wieczorek GF (2005) Calibration of numerical models for small debris flows in Yosemite Valley, California, USA. Nat Hazards Earth Syst Sci 5(6):993–1001. https://doi.org/10.5194/nhess-5-993-2005

Bigano A, Pauli F (2007) Dimensioni socio-economiche, costi dell’inflazione e strategie di adattamento per l’impatto del cambiamento climatico sul sistema idrogeologico italiano. In Report prepared for the APAT Workshop on “Cambiamenti climatici e dissesto idrogeologico: scenari futuri per un programma nazionale di adattamento”, Napoli (pp. 9-10)

Bolognini G, Soto MA, Di Pasquale F (2009) Fiber-optic distributed sensor based on hybrid Raman and Brillouin scattering employing multiwavelength Fabry–Pérot lasers. IEEE Photonics Technology Letters 21(20):1523-1525

Butler DR, Malanson GP (1992) Effects of terrain on excessive travel distance by snow avalanches. Northwest science 66(2):77-85.

Coviello V, Arattano M, Comiti F, Macconi P, Marchi L (2019) Seismic characterization of debris flows: Insights into energy radiation and implications for warning. Journal of Geophysical Research: Earth Surface 124:1440–1463. https://doi.org/10.1029/2018JF004683

Edme P, Paitz, P, Walter F, van Herwijnen A, Fichtner A (2023) Fiber-optic detection of snow avalanches using telecommunication infrastructure. arXiv preprint arXiv:2302.12649

EEA (2017) Climate change adaptation and disaster risk reduction in Europe 2017. EEA Report No 15/2017, Publications Office of the European Union, Luxembourg, 2017, pp 172. https://doi.org/10.2800/938195

Fichtner A, Klaasen S, Thrastarson S, Cubuk-Sabuncu Y, Paitz P, Jonsdottir K (2022) Fiber-optic observation of volcanic tremor through floating ice-sheet resonance. The Seismic Record 2(3):148-155. https://doi.org/10.1785/0320220010

Forman PR, Jahoda FC (1988) Linear birefringence effects on fiber-optic current sensors. Appl. Opt. 27(15):3088-3096. https://doi.org/10.1364/AO.27.003088

Gauer P (2014) Comparison of avalanche front velocity measurements and implications for avalanche models. Cold regions science and technology 97:132-150. https://doi.org/10.1016/j.coldregions.2013.09.010

Gauer P, Kern M, Kristensen K, Lied K, Rammer L, Schreiber H (2007) On pulsed Doppler radar measurements of avalanches and their implication to avalanche dynamics. Cold Regions Science and Technology 50(1-3):55-71. https://doi.org/10.1016/j.coldregions.2007.03.009

Havens S, Marshall HP, Johnson JB, Nicholson B (2014) Calculating the velocity of a fast-moving snow avalanche using an infrasound array. Geophysical Research Letters 41(17):6191-6198. https://doi.org/10.1002/2014GL061254

Hong CY, Zhang YF, Zhang MX, Leung LMG, Liu LQ (2016) Application of FBG sensors for geotechnical health monitoring, a review of sensor design, implementation methods and packaging techniques. Sensors and Actuators A: Physical 244:184-197. https://doi.org/10.1016/j.sna.2016.04.033

Hudson TS, Baird AF, Kendall JM, Kufner SK, Brisbourne AM, Smith AM, Butcher A, Chalari A, Clarke A (2021) Distributed Acoustic Sensing (DAS) for natural microseismicity studies: A case study from Antarctica. J. Geophys. Res.: Solid Earth 126, e2020JB021493. https://doi.org/10.1029/2020JB021493

Hungr O, Leroueil S, Picarelli L (2014) The Varnes classification of landslide types, an update. Landslides 11:167-194. https://doi.org/10.1007/s10346-013-0436-y

Hurlimann M, Rickenmann D, Graf C (2003) Field and monitoring data of debris-flow events in the Swiss Alps. Canadian Geotechnical Journal 40:161–175. https://doi.org/10.1139/t02-087

Hürlimann M, Coviello V, Bel C, Guo X, Berti M, Graf C, Hübl J, Miyata S, Smith JB, Yin HY (2019) Debris-flow monitoring and warning: Review and examples. Earth-Science Reviews 199, 102981. https://doi.org/10.1016/j.earscirev.2019.102981

Inaudi D (2014) Sensing solutions for assessing the stability of levees, sinkholes and landslides. In: Sensor Technologies for Civil Infrastructures; Elsevier: Amsterdam, The Netherlands, 2014; Volume 1

Insana A, Beroya-Eitner MA, Barla M, Zachert H, Žlender B, van Marle M, Kalsnes B, Bracko T, Pereira C, Prodan I, Szymkiewicz F, Löfroth H (2021) Climate Change Adaptation of Geo-Structures in Europe: Emerging Issues and Future Steps. Geosciences 11(12), 488.

IPCC (2023) Climate change 2023. Synthesis Report. The Intergovernmental Panel on Climate Change, 169 pp. https://doi.org/10.59327/IPCC/AR6-9789291691647

Itakura Y, Inaba H, Sawada T (2005) A debris-flow monitoring devices and methods bibliography. Nat. Hazards Earth Syst. Sci. 5(6):971-977. https://doi.org/10.5194/nhess-5-971-2005, 2005.

Iverson RM (1997) The physics of debris flows. Rev Geophys 35(3):245–296. https://doi.org/10.1029/97RG00426

Jakob M (2005) A size classification for debris flows. Engineering geology 79(3-4):151-161. https://doi.org/10.1016/j.enggeo.2005.01.006

Johansson S, Farhadiroushan M, Parker T (2000) Application of fibre-optics systems in embankment dams for temperature, strain and pressure measurements-Some comparisons and experiences. In: Transactions of the International Congress on Large Dams. 2000. p. 1125-1146

Kogelnik H, Winzer PJ (2012) Modal birefringence in weakly guiding fibers. Journal of Lightwave Technology 30(14):2240–2245. https://doi.org/10.1109/JLT.2012.2193872

Leonardi A, Pirulli M, Barbero M, Barpi F, Borri-Brunetto M, Pallara O, Segor V (2021) Impact of Debris Flows on Filter Barriers: Analysis Based on Site Monitoring Data. Environmental & Engineering Geoscience 27(2):195–212. https://doi.org/10.2113/eeg-d-20-00013

Lloret S, Rastogi P, Thévenaz L, Inaudi D (2003) Measurement of dynamic deformations using a path-unbalance Michelson-interferometer-based optical fiber sensing device. Opt. Eng. 42(3):662–669

Marchi L, Arattano M, Deganutti AM (2002) Ten years of debris-flow monitoring in the Moscardo Torrent (Italian Alps). Geomorphology 46(1-2):1-17. https://doi.org/10.1016/S0169-555X(01)00162-3

McClung D, Schaerer PA (2006). The avalanche handbook. The Mountaineers Books

Michlmayr G, Chalari A, Clarke A, Or D (2017) Fiber-optic high-resolution acoustic emission (AE) monitoring of slope failure. Landslides 14(3):1139-1146. https://doi.org/10.1007/s10346-016-0776-5

Motil A, Bergman A, Tur M (2016) State of the art of Brillouin fiber-optic distributed sensing. Optics & Laser Technology 78:81-103. https://doi.org/10.1016/j.optlastec.2015.09.013

Nagl G, Hübl J, Kaitna R (2022). Stress anisotropy in natural debris flows during impacting a monitoring structure. Landslides 19:211–220. https://doi.org/10.1007/s10346-021-01779-2

Olivero M, Insana A, Vallan A, Gaudino R, Barla M, Perrone G (2018) Fibre Bragg Gratings Monitoring in a Pilot Project of an Energy Tunnel, 20th Italian National Conference on Photonic Technologies (Fotonica 2018), Lecce, Italy, 2018, pp. 1-4. https://doi.org/10.1049/cp.2018.1649

Pelfini M, Santilli M (2008) Frequency of debris flows and their relation with precipitation: A case study in the Central Alps, Italy. Geomorphology 101(4):721-730

Pellegrini S, Rizzelli G, Barla M, Gaudino R (2023) Algorithm Optimization for Rockfalls Alarm System Based on Fiber Polarization Sensing. IEEE PHOTONICS JOURNAL 15(3):1-9. https://doi.org/10.1109/JPHOT.2023.3281670

Pellegrini, S, Rizzelli, G., Barla M., Gaudino R. (2024) Polarization-Based Fiber Optic System for Debris Flow Early Warning: On-Field Demonstration. IEEE PHOTONICS JOURNAL 16(3): 1-8. https://doi.org/10.1109/JPHOT.2024.3403159

Prochaska AB, Santi PM, Higgins JD, Cannon SH (2008) A study of methods to estimate debris flow velocity. Landslides 5(4):431-444. https://doi.org/10.1007/s10346-008-0137-0

Qin, J.-Q., Yin J.-H., Zhu Z.-H., Tan D.-Y. (2020) Development and application of new FBG mini tension link transducers for monitoring dynamic response of a flexible barrier under impact loads. Measurement 153 (2020) 107409. https://doi.org/10.1016/j.measurement.2019.107409

Rammer L, Kern MA, Gruber U, Tiefenbacher F (2007) Comparison of avalanche-velocity measurements by means of pulsed Doppler radar, continuous wave radar and optical methods. Cold Regions Science and Technology 50(1-3):35-54. https://doi.org/10.1016/j.coldregions.2007.03.014

Sass O, Oberlechner M (2012) Is climate change causing increased rockfall frequency in Austria? Natural Hazards and Earth System Sciences 12(11):3209-3216. https://doi.org/10.5194/nhess-12-3209-2012

Schenato L (2017) A review of Distributed Fibre Optic Sensors for Geo-Hydrogeological applications. Appl. Sci. 7(9):896. https://doi.org/10.3390/app7090896

574 Schimmel A, Coviello V, Comiti F (2022) Debris flow velocity and volume estimations based on seismic data. Nat. Hazards
575 Earth Syst. Sci. 22:1955–1968. https://doi.org/10.5194/nhess-22-1955-2022

576 Schweizer J, Bartelt P, van Herwijnen A (2021) Chapter 12 - Snow avalanches. In: Snow and ice-related hazards, risks,
577 and disasters (Second Edition), edited by: Haeberli, W. and White- man, C., Elsevier, 377–416.
578 https://doi.org/10.1016/B978-0-12-394849-6.00012-3

579 Stocker TF et al. (eds) (2013) Climate Change 2013: The Physical Science Basis. Cambridge Univ. Press, 2013

580 Stoffel M, Huggel C (2012) Effects of climate change on mass movements in mountain environments. Progress in physical
581 geography 36(3):421-439. https://doi.org/10.1177/0309133312441010

582 Tan D. -Y., Yin J.-H., Qin J.-Q., Zhu Z.-H., Feng W.-Q. (2020) Experimental study on impact and deposition behaviours of
583 multiple surges of channelized debris flow on a flexible barrier. Landslides (2020) 17:1577–1589.
584 https://doi.org/10.1007/s10346-020-01378-7

585 Thüring T, Schoch M, van Herwijnen A, Schweizer J (2015) Robust snow avalanche detection using supervised machine
586 learning with infrasonic sensor arrays. Cold Regions Science and Technology 111:60-66

587 Ulivieri G, Marchetti E, Ripepe M, Chiambretti I, De Rosa G, Segor V (2011) Monitoring snow avalanches in Northwestern
588 Italian Alps using an infrasound array. Cold Regions Science and Technology 69(2-3):177-183

589 Wang H, Guo J-K, Mo H, Zhou X, Han Y (2023). Fiber Optic Sensing Technology and Vision Sensing Technology for
590 Structural Health Monitoring. Sensors 23(9), 4334. https://doi.org/10.3390/s23094334
591 Zhu HH, Shi B, Zhang CC (2017) FBG-Based Monitoring of Geohazards: Current Status and Trends. Sensors 17(3), 452.
592 https://doi.org/10.3390/s17030452